# Spontaneous symmetry breaking in a split potential box

Elad Shamriz,[1] Nir Dror,[1] and Boris A. Malomed[1,2]
[1]*Department of Physical Electronics, School of Electrical Engineering, Faculty of Engineering, Tel Aviv University, Tel Aviv 69978, Israel*
[2]*Laboratory of Nonlinear-Optical Informatics, ITMO University, St. Petersburg 197101, Russia*
(Received 30 January 2016; published 12 August 2016)

We report results of an analysis of the spontaneous symmetry breaking (SSB) in a basic (actually, simplest) model that is capable of producing the SSB phenomenology in a one-dimensional setting. It is based on the Gross-Pitaevskii–nonlinear Schrödinger equation with the cubic self-attractive term and a double-well potential built as an infinitely deep potential box split by a narrow ($\delta$ functional) barrier. The barrier's strength $\varepsilon$ is the single free parameter of the scaled form of the model. It may be implemented in atomic Bose-Einstein condensates and nonlinear optics. The SSB bifurcation of the symmetric ground state (g.s.) is predicted analytically in two limit cases, viz., for deep or weak splitting of the potential box by the barrier ($\varepsilon \gg 1$ or $\varepsilon \ll 1$, respectively). For the generic case, a variational approximation (VA) is elaborated. The analytical findings are presented along with systematic numerical results. The stability of stationary states is studied through the calculation of eigenvalues for small perturbations and by means of direct simulations. The g.s. always undergoes the SSB bifurcation of the supercritical type, as predicted by the VA at moderate values of $\varepsilon$, although the VA fails at small $\varepsilon$, due to inapplicability of the underlying ansatz in that case. However, the latter case is correctly treated by the approximation based on a soliton ansatz. On top of the g.s., the first and second excited states are studied too. The antisymmetric mode (the first excited state) is destabilized at a critical value of its norm. The second excited state undergoes SSB bifurcation, like the g.s., but, unlike it, the bifurcation produces an unstable asymmetric mode. All unstable modes tend to spontaneously reshape into the asymmetric g.s.

DOI: 10.1103/PhysRevE.94.022211

## I. INTRODUCTION AND MODEL

The dynamics of confined collective excitations in nonlinear physical systems, modeled by one or several fields, is determined by the interplay of the field-trapping potential and the character of interactions of the field(s). In particular, the system's spatial symmetry is determined by the shape of the potential. A generic type of the latter is represented by double-well potentials (DWPs), which feature symmetry between two wells separated by a barrier.

In quantum mechanics [1] and linear field theories mathematically similar to it, such as paraxial light propagation in linear optical waveguides [2], the ground state (g.s.) of a confined system normally follows the symmetry of the trapping potential (the Jahn-Teller effect in molecules exemplifies another possibility, when the g.s. of the electron wave function in the complex system is spatially asymmetric, thus breaking the symmetry of the full Hamiltonian [3]). Other representations of the same symmetry may be realized by the system's excited states. Thus, the g.s. wave function trapped in the one-dimensional DWP is symmetric (even) with respect to the double-well structure, while the first excited state is antisymmetric (odd).

Unlike the linear quantum-mechanical Schrödinger equation for a single particle, atomic Bose-Einstein condensates (BECs) are modeled by the Gross-Pitaevskii equation (GPE) for the single-atom wave function $\psi(x,t)$, with a trapping potential $U(x)$ and a cubic term that accounts for collisions between atoms, in the framework of the mean-field approximation [4]:

$$i\frac{\partial \psi}{\partial t} = -\frac{1}{2}\frac{\partial^2 \psi}{\partial x^2} - g|\psi|^2\psi + U(x)\psi. \tag{1}$$

This equation is written in the scaled form, which can be derived from the three-dimensional GPE for the cigar-shaped configuration, with strong confinement applied in the transverse plane [5]. The repulsive or attractive interactions between atoms correspond, respectively, to the self-defocusing ($g < 0$) or self-focusing ($g > 0$) sign of the cubic term in Eq. (1). Similarly, the nonlinear Schrödinger equation (NLSE) with the cubic term governs the paraxial propagation of electromagnetic waves in optical media with Kerr nonlinearity [6]. In the latter case, Eq. (1) applies to the light transmission in the spatial domain, with $t$ replaced by the propagation distance $z$ and $-U(x)$ representing a transverse modulation profile of the local refractive index, which imposes a guiding structure in the $(x,z)$ plane.

Many models of nonlinear optics and BEC are based on the GPE-NLSE in the form of Eq. (1) with the potential $U(x)$ representing symmetric DWPs. A fundamental difference from the linear systems is that the g.s. in the self-focusing models follows the symmetry of the underlying potential structure only if the nonlinearity remains relatively weak. A generic effect, which occurs with an increase of the strength of the nonlinearity as a result of its interplay with the DWP, is spontaneous symmetry breaking (SSB), which destabilizes the symmetric g.s. and replaces it with an asymmetric one [7]. The switch from the symmetric g.s. to its asymmetric counterpart occurs via the corresponding *bifurcation* (phase transition) at a critical value of the nonlinearity strength [8,9].

Originally, the SSB was predicted in simple models based on systems of linearly coupled equations with intrinsic nonlinearity [10]. In particular, Eq. (1) with the potential $U(x)$ in the form of two symmetric deep wells can be reduced to a system of two coupled ordinary differential equations for amplitudes $u_1(t)$ and $u_2(t)$ in the framework of the tight-binding approximation [11], which replaces $\psi(x,t)$

 

with a superposition of two stationary wave functions $\phi$, corresponding to the states trapped separately in the two deep potential wells, centered at $x = \pm a$:

$$\psi(x,t) = u_1(t)\phi(x-a) + u_2(t)\phi(x+a). \tag{2}$$

In terms of the BEC, the SSB gives rise to the g.s. with the atomic density in one well of the trapping DWP larger than in the other. The SSB also breaks another principle of quantum mechanics, according to which the g.s. cannot be degenerate, as there emerges a degenerate pair of mirror-image asymmetric g.s. wave functions, with the larger density self-trapped in either of the two potential wells. In optics, the SSB means that higher light power spontaneously self-traps in either core of the nonlinear dual-core waveguide.

Thus, the SSB effect is common to diverse systems that combine the wave transmission, self-focusing, and trapping potentials of the DWP type. In photonics, the SSB was reported in several experimental works. In particular, the symmetry breaking for a pair of laser beams coupled into a transverse DWP created in a self-focusing photorefractive medium was demonstrated in Ref. [12]. Another experimental result is a spontaneously established asymmetric regime of the operation of a symmetric pair of coupled lasers [13]. More recently, SSB was demonstrated in a pair of nanolaser cavities embedded in a photonic crystal [14]. Observation of spontaneous breaking of the chiral symmetry in metamaterials was reported in Ref. [15].

The analysis of the SSB in the model based on Eq. (1) was initiated in Refs. [16,17]. Most often, the BEC nonlinearity (in contrast to the self-focusing Kerr effect in optics) is self-repulsive, which corresponds to $g < 0$ in Eq. (1). In this case, the symmetric (even) g.s. is not subject to destabilization, but the first antisymmetric (odd) excited state, with $\psi(-x) = -\psi(x)$, suffers destabilization and spontaneous breakup of its antisymmetry when the strength of the repulsive nonlinearity attains a critical level [7]. This manifestation of the SSB phenomenology was demonstrated experimentally in Ref. [18], using the condensate of $^{87}$Rb atoms with repulsive interactions between them, loaded into a DWP trapping configuration.

The above discussion addressed static symmetric and asymmetric modes in the nonlinear systems including the DWP structure. Dynamical regimes, in the form of oscillations of the wave function between two wells of the DWP, i.e., roughly speaking, between the two mirror-image asymmetric states existing above the SSB point, were studied too. Following the analogy to Josephson oscillations in tunnel-coupled superconductors [19,20], the possibility of the matter-wave oscillations in *bosonic Josephson junctions* was predicted [21] and experimentally realized in the trapped BEC [18].

Additional dynamical regimes were studied in Ref. [22], in the framework of a model that combines the DWP and nonlinearity management, i.e., time-periodic modulation of coefficient $g$ in Eq. (1). It was demonstrated that the symmetry-breaking dynamics may be strongly altered by the application of the management: The SSB can be suppressed in cases when it occurs and induced in cases when it does not take place in the absence of the management.

The objective of the present work is to explore, by means of analytical and numerical methods, the SSB in a fundamental version of the systems represented by Eq. (1) with the self-attractive nonlinearity ($g > 0$), namely, an infinitely deep potential box (whose width is scaled to be 1), split in two wells by a narrow barrier, as schematically shown in Fig. 1. In this case, Eq. (1) with the barrier represented by the ideal $\delta$ function takes the form of the following equation subject to zero boundary conditions:

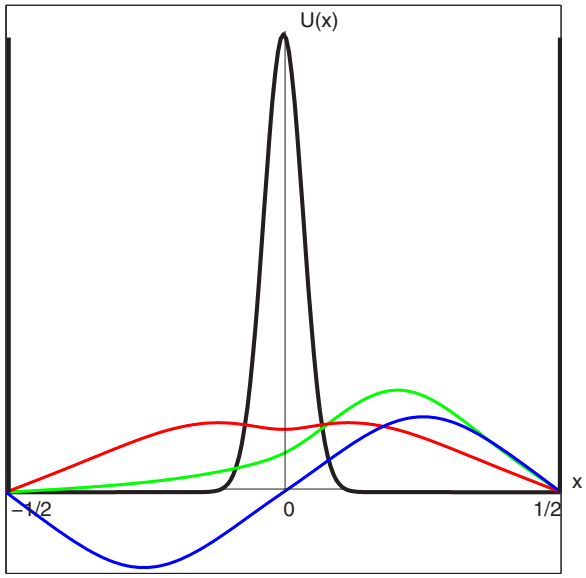


FIG. 1. Setting under consideration. An infinitely deep potential box of width 1 is split in the middle by a narrow tall barrier, approximated by $U(x) = \varepsilon\delta(x)$ [see Eq. (3)]. Wave functions of symmetric (even), antisymmetric (odd), and asymmetric stationary states are schematically shown by red, blue, and green curves, respectively.

$$i\frac{\partial\psi}{\partial t} = -\frac{1}{2}\frac{\partial^2\psi}{\partial x^2} - g|\psi|^2\psi + \varepsilon\delta(x)\psi, \tag{3}$$

$$\psi\left(x = \pm\tfrac{1}{2}\right) = 0, \tag{4}$$

where $\varepsilon > 0$ is the strength of the splitter and $g = 1$ may be fixed, unless $g = 0$ is set in the linear version of Eq. (3). The Hamiltonian (energy) corresponding to Eqs. (3) and (4) is

$$H = \frac{1}{2}\int_{-1/2}^{+1/2}\left(\left|\frac{\partial\psi}{\partial x}\right|^2 - |\psi|^4\right)dx + \varepsilon|\psi(x=0)|^2. \tag{5}$$

In a sense, this model is opposite to the one introduced in recent work [23], in which the SSB was studied in a DWP with an elevated floor (rather than the infinitely deep one), i.e., a DWP structure embedded into a broad potential barrier.

It is relevant to mention that, although the one-dimensional NLSE is integrable in the free space, the internal potential and boundary conditions in Eqs. (3) and (4) destroy the integrability, therefore the evolution of unstable states in this model is not expected to be periodic or quasiperiodic in time [see Figs. 12 and 15(c) below as examples]. The model gives rise to nearly integrable dynamics only in the case when the solution may be approximated by a set of narrow solitons (this case is considered in Sec. II C). It may be expected that the dynamics reduced to the variational approximation (VA), based on the ansatz (29) with three degrees of freedom, may be close to quasiperiodic, as the presence of two dynamical

invariants, viz., the norm, given by Eq. (30), and the respective Hamiltonian, makes the approximate dynamical system nearly integrable, with quasiperiodic trajectories carried by Kolmogorov-Arnold-Moser tori [24]. Actually, our VA-based analysis is focused below on its stationary version, which is most essential in terms of the present work. On the other hand, it should be stressed that the nonintegrable dynamics remains reversible [24], as the model does not include any dissipation.

In spite of the fact that Eqs. (3)–(5) present, as a matter of fact, the simplest version of model (1), it was introduced only recently in Refs. [25,26] (where some analytical approximations were introduced, but systematic analysis was not performed). The model can be implemented in BECs, using strong repelling optical sheets to emulate both the outer potential walls and the inner barrier, the widths of the latter and of the whole potential box being, respectively, $\sim 1$ $\mu$m and $\sim 100$ $\mu$m in physical units. In optics, the box structure may be realized as a step-index one made in silica [2,27]. Assuming the width of the waveguide $\sim 20$ $\mu$m (to have it narrow enough for potential applications), characteristic values of interest, $\varepsilon \sim 10$ (see below), correspond to the splitting layer of thickness $\sim 2$ $\mu$m.

The rest of the paper is organized as follows. An analytical approach to the model is recapitulated in Sec. II, following its (incomplete) introduction in Ref. [26], which is necessary for comparison with numerical results. The analysis includes the VA for stationary symmetric and asymmetric modes, as well as approximations for weakly and strongly split potential boxes, i.e., small and large $\varepsilon$, in terms of Eq. (3). Results of systematic numerical studies and a comparison with analytical predictions are reported in Sec. III, which demonstrates that the VA is quite accurate for the model with a relatively tall splitting barrier ($\varepsilon$ not too small), while the VA yields a wrong bifurcation diagram for small $\varepsilon$, due to inadequacy of the underlying ansatz (when, however, the other analytical approximation, based on the soliton ansatz, applies correctly). The numerical results are reported for symmetric, asymmetric, and antisymmetric bound states (the latter representing the first excited state in the system), including simulations of dynamical regimes initiated by the SSB instability of symmetric and antisymmetric ones. The paper is summarized in Sec. IV.

## II. ANALYTICAL APPROACH

### A. Stationary modes

Stationary states produced by Eqs. (3) and (4) with real energy eigenvalue $\mu$ (in terms of optics, $-\mu$ is the propagation constant) are sought as

$$\psi(x,t) = e^{-i\mu t}\phi(x), \tag{6}$$

with the real wave function $\phi(x)$ obeying a stationary equation with the respective boundary condition (BC):

$$\mu\phi = -\frac{1}{2}\frac{d^2\phi}{dx^2} - g\phi^3 + \varepsilon\delta(x)\phi, \phi\left(x = \pm\frac{1}{2}\right) = 0. \tag{7}$$

The presence of the $\delta$-functional barrier at $x = 0$ implies that $\phi(x)$ is continuous at this point, while its derivative obeys a jump condition

$$\left.\frac{d\phi}{dx}\right|_{x=+0} - \left.\frac{d\phi}{dx}\right|_{x=-0} = 2\varepsilon\phi(x=0). \tag{8}$$

As mentioned above, $g \equiv 1$ is fixed throughout the paper, unless $g = 0$ is set in the linear case; hence the strength of the nonlinearity is determined by the norm of the wave function

$$N = \left(\int_{-1/2}^{0} + \int_{0}^{+1/2}\right)\phi^2(x)dx \equiv N_- + N_+. \tag{9}$$

The asymmetry of states above the SSB point is characterized by the relative difference of the norms in the right and left sections of the split potential box

$$\Theta \equiv (N_+ - N_-)/(N_+ + N_-). \tag{10}$$

Before proceeding to the consideration of the nonlinear model, it is relevant to dwell on its linear counterpart, with $g = 0$ in Eq. (7). Spatially symmetric (even) solutions of the linear equation are sought as

$$\phi^{(\mathrm{lin})}_{\mathrm{even}}(x) = A\sin\left[\sqrt{2\mu}\left(\tfrac{1}{2} - |x|\right)\right], \tag{11}$$

where $A$ is an arbitrary amplitude and eigenvalue $\mu$ is determined by a relation following from Eq. (8):

$$\tan(\sqrt{\mu/2}) = -\sqrt{2\mu}/\varepsilon. \tag{12}$$

It is easy to see that, with the increase of $\varepsilon$ from 0 to $\infty$, the lowest eigenvalue $\mu_0$, which corresponds to the g.s. of the linear model, monotonically grows from $\mu_0(\varepsilon = 0) = \pi^2/2$ to

$$\mu_0(\varepsilon = \infty) = 2\pi^2. \tag{13}$$

Similarly, the eigenvalue of the first excited symmetric state $\mu_2(\varepsilon)$ monotonically grows from $\mu_2(\varepsilon = 0) = 9\pi^2/2$ to $\mu_2(\varepsilon = \infty) = 8\pi^2$. The eigenvalue $\mu_1 = 2\pi^2$, which corresponds to the lowest excited state, i.e., the first antisymmetric (odd) eigenfunction,

$$\phi^{(\mathrm{lin})}_{\mathrm{odd}}(x) = A\sin(\sqrt{2\mu_1}x) \tag{14}$$

[$\mu_1$ does not depend on $\varepsilon$, as the wave function (14) vanishes at $x = 0$], is located between $\mu_0$ and $\mu_2$. Naturally, $\mu_1$ coincides with the limit value (13) of $\mu_0$, as the g.s. eigenfunction also vanishes at $x = 0$, in the limit of $\varepsilon = \infty$.

### B. Deeply split double-well potential (large $\varepsilon$)

The first objective of the analysis of the nonlinear model based on Eq. (7) is to predict the critical norm at the SSB point. In the case of weakly coupled (deeply split) potential wells, which corresponds to large $\varepsilon$ (a very tall splitting barrier), weak nonlinearity, which corresponds to a small norm and amplitude of the wave function, is sufficient to induce the SSB in the competition with the weak linear coupling. The small amplitude implies that relevant solutions to Eq. (7) are close to the eigenmodes (11) of the linear equation, hence an approximate solution may be sought as

$$\phi(x) = A_\pm\sin\left[k_\pm\left(\tfrac{1}{2} - |x|\right)\right], \tag{15}$$

where the signs $\pm$ pertain to $x < 0$ and $x > 0$, respectively. The substitution of this ansatz into the condition of the continuity of the wave function at $x = 0$ and the relation (8) for its

first derivative leads to the following relations between the amplitudes $A_\pm$ and the wave numbers:

$$A_+ \sin\left(\tfrac{1}{2}k_+\right) = A_- \sin\left(\tfrac{1}{2}k_-\right), \tag{16}$$

$$A_- k_- \cos\left(\tfrac{1}{2}k_-\right) - A_+ k_+ \cos\left(\tfrac{1}{2}k_+\right) = 4\varepsilon A_\pm \sin\left(\tfrac{1}{2}k_\pm\right). \tag{17}$$

In the same small-amplitude approximation, the third harmonic contained in the cubic term in Eq. (7) may be neglected, hence this term is approximated as

$$\left\{A_\pm \sin\left[k_\pm\left(\tfrac{1}{2} - |x|\right)\right]\right\}^3 \approx \tfrac{3}{4}A_\pm^3 \sin\left[k_\pm\left(\tfrac{1}{2} - |x|\right)\right]. \tag{18}$$

Further, Eq. (18) implies that the cubic term amounts to an effective shift of the energy eigenvalue in Eq. (7), which determines the wave numbers in Eq. (15):

$$k_\pm = \sqrt{2\left(\mu + \tfrac{3}{4}gA_\pm^2\right)}. \tag{19}$$

In the limit of $\varepsilon \to \infty$, the wave functions (15) must vanish at $x = 0$, hence the respective g.s. corresponds to $k_\pm = 2\pi$. At large but finite $\varepsilon$, the energy corresponding to the g.s. should be close to the limit value given by Eq. (13),

$$\mu = 2\pi^2 - \delta\mu, \quad \delta\mu \ll 2\pi^2. \tag{20}$$

The substitution of the expression (20) into Eq. (19), expanding it for small $\delta\mu$ and $A_\pm^2$, inserting the result into Eqs. (16) and (17), and taking the limit of $A_+ - A_- \to 0$, which corresponds to the SSB bifurcation point, leads to the following analytical prediction for the bifurcation-point parameters:

$$N_{\rm bif} = \tfrac{8}{3}\pi^2\varepsilon^{-1}, \quad (A_\pm^2)_{\rm bif} = 2N_{\rm cr}, \quad \delta\mu = 12\pi^2\varepsilon^{-1}. \tag{21}$$

Thus, as expected, the value of the norm at the SSB point decays ($\sim\varepsilon^{-1}$) with an increase of $\varepsilon$. This approximate analytical result is compared with its numerical counterpart in Fig. 2(a) (the numerical results are presented in the next section).

### C. Weakly split double-well potential (small $\varepsilon$)

Small $\varepsilon$ implies strong coupling of the two potential wells with a shallow split between them, therefore strong nonlinearity, i.e., large $N$, is required to cause the SSB under the competition with the strong coupling. In turn, large $N$ implies that the wave field tends to self-trap into a narrow NLSE soliton [6],

$$\phi_{\rm sol}(x - \xi) = \tfrac{1}{2}N\,\mathrm{sech}\left[\tfrac{1}{2}N(x - \xi)\right], \tag{22}$$

where $\xi$ is the coordinate of the soliton's center, the respective energy eigenvalue being

$$\mu_{\rm sol} = -N^2/8. \tag{23}$$

This approximation is valid provided the soliton's width is much smaller than the size of the potential box, which means $N \gg 1$.

According to the BC in Eq. (7), the soliton interacts with two *ghost solitons*, i.e., its mirror images (with opposite signs), with respect to the edges of the box:

$$\phi_{\rm ghost}(x) = -\frac{N}{2}\left[\mathrm{sech}\left(\frac{1}{2}N(x - 1 + \xi)\right) + \mathrm{sech}\left(\frac{1}{2}N(x + 1 + \xi)\right)\right]. \tag{24}$$

The sum of the well-known potentials [28,29] of the interaction of the given soliton with the two ghosts gives rise to an effective potential of repulsion of the real soliton from edges of the confining box:

$$U_{\rm box}(\xi) = N^3 \exp(-N/2)\cosh(N\xi). \tag{25}$$

On the other hand, the same soliton is repelled by the splitting barrier, with the corresponding potential [29]

$$U_{\rm barrier}(\xi) = \varepsilon\phi_{\rm sol}^2(\xi = 0) = \frac{\varepsilon}{4}N^2\mathrm{sech}^2\left(\frac{1}{2}N\xi\right), \tag{26}$$

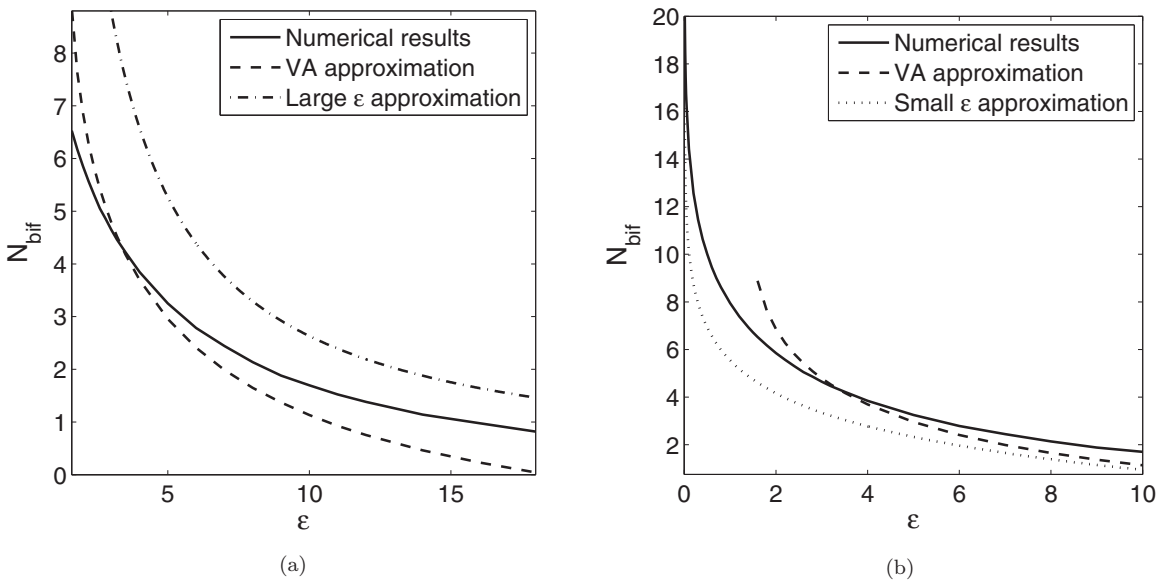


(a) (b)

FIG. 2. Norm at the symmetry-breaking bifurcation point versus the strength of the splitting barrier $\varepsilon$. Along with the numerically found and VA-predicted dependences, shown are the analytical approximations based on (a) Eq. (21) and (b) Eq. (27), which are relevant, respectively, for large and small $\varepsilon$ [note that in (a) the range starts from $\varepsilon \approx 2.7$].

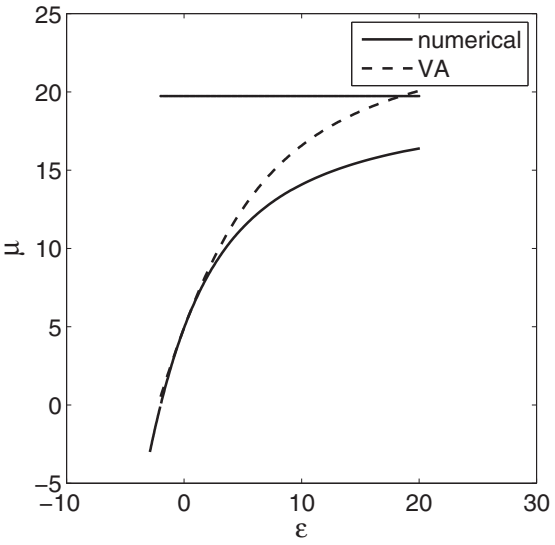


FIG. 3. Eigenvalue for the energy of the g.s. in the linear version of Eq. (7) ($g = 0$) versus the strength of the splitting barrier $\varepsilon$ as obtained from the numerical solution of Eq. (12) and as predicted by the VA in the form of Eq. (39). The horizontal line shows the constraint imposed by Eq. (13).

if the deformation of the soliton's shape by the weak barrier is neglected. A straightforward analysis of the total effective potential $U(\xi) = U_{\rm box}(\xi) + U_{\rm barrier}(\xi)$ demonstrates that the position of the soliton placed at $\xi = 0$, which represents the symmetric mode in the present case, is stable, i.e., it corresponds to a *minimum* of the net potential, at $8N\exp(-N/2) > \varepsilon$ or, in other words, at

$$N < N_{\rm bif} \approx 2\ln(16/\varepsilon). \tag{27}$$

The SSB bifurcation takes place, with an increase of $N$, at $N = N_{\rm bif}$, when the local potential minimum at $\xi = 0$ switches into a maximum. At $0 < (N - N_{\rm bif})/N_{\rm bif} \ll 1$, the center of the soliton spontaneously shifts to either of two asymmetric positions, which correspond to a pair of new potential minima emerging at $\xi = \pm\sqrt{(N - N_{\rm bif})}/N_{\rm cr}$.

A comparison of the approximate analytical result given by Eq. (27) with its numerically obtained counterpart is displayed in Fig. 2(b). At moderate values of $\varepsilon$ the discrepancy is relatively large because the validity condition for the present approximation is that $\varepsilon$ must be so small that $\ln(16/\varepsilon)$ may be treated as a large parameter.

### D. Variational approximation

In the generic case, when the strength of the splitting barrier $\varepsilon$ is not assumed to be specifically large or small, an analytical consideration may be based on the VA [30], which is suggested by the fact that the stationary equation (7) may be derived from the minimization of the corresponding Lagrangian,

$$L = \int_{-1/2}^{+1/2} \left[\frac{1}{2}\left(\frac{d\phi}{dx}\right)^2 - \mu\phi^2 - \frac{g}{2}\phi^4\right]dx + \varepsilon\phi^2(x=0)$$
$$\equiv H - \mu N, \tag{28}$$

where $H$ and $N$ are the Hamiltonian (5) and norm (9) defined above. The following ansatz for the g.s. wave function, satisfying the BC in Eq. (7), is the simplest one that is capable of capturing the SSB:

$$\phi(x) = a\cos(\pi x) + b\sin(2\pi x) + c\cos(3\pi x) \tag{29}$$

[cf. Eq. (2)], where the real amplitudes $a$, $c$, and $b$ must be predicted by the VA. The SSB is accounted for by the odd term $\sim b$ in the ansatz, which breaks the symmetry of the even expression. Accordingly, the onset of the SSB is signaled by the emergence of a solution with infinitesimal $b$, branching off from from the symmetric one with $b = 0$.

The integral norm (9) of the ansatz (29) is

$$N = (1/2)(a^2 + c^2 + b^2), \tag{30}$$

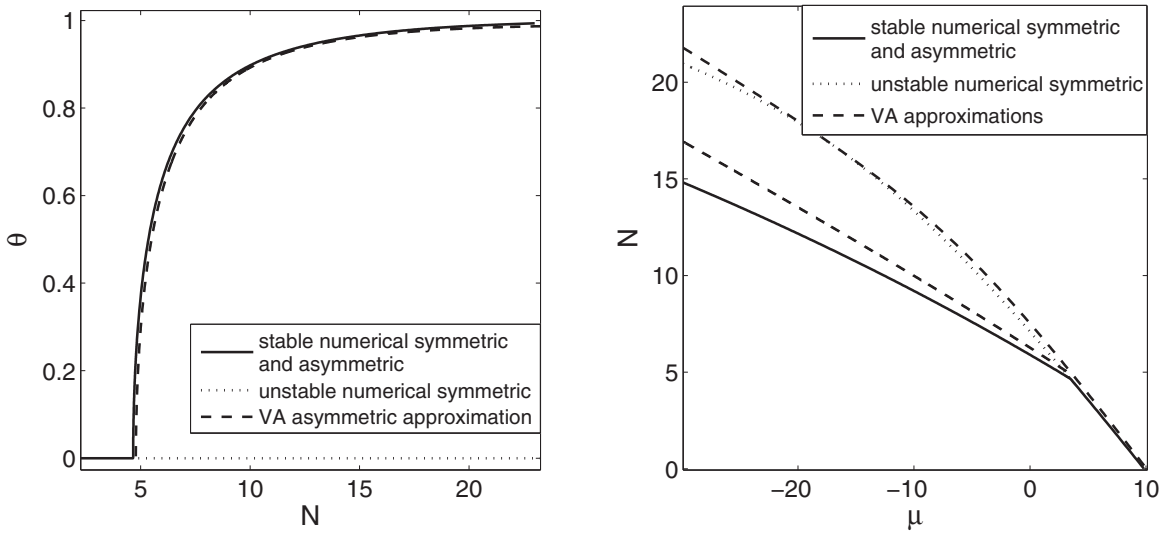


(a) (b)

FIG. 4. (a) Asymmetry of the stationary solutions, defined as per Eqs. (9) and (10), as a function of the total norm, at $\varepsilon = 3$. For the VA solution, the asymmetry is calculated through Eq. (31). (b) Dependence between the total norm and energy eigenvalue for the same solutions.

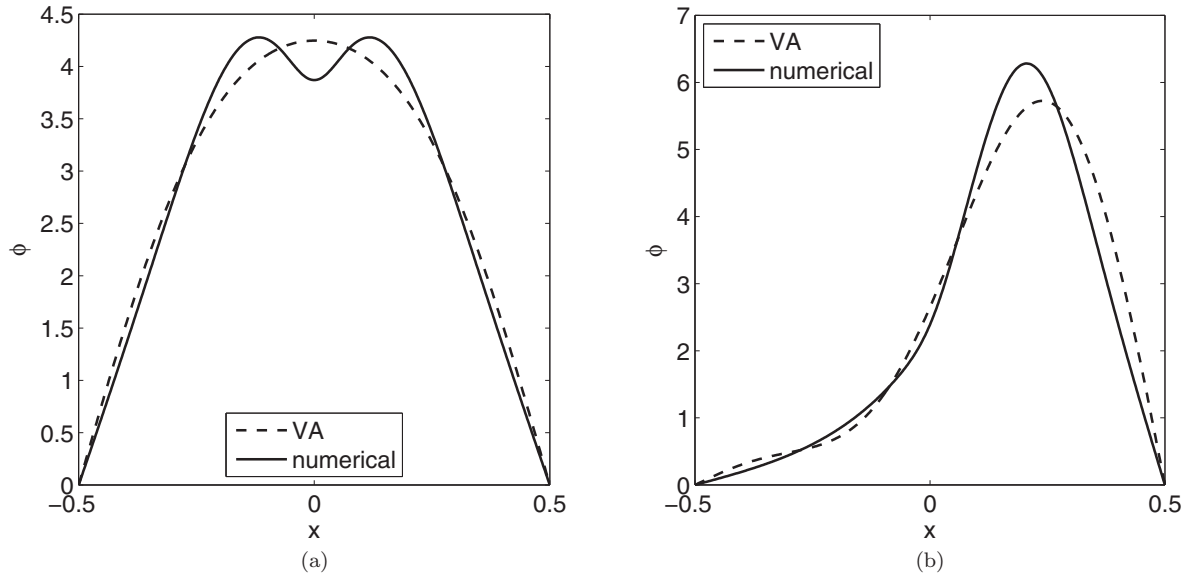


FIG. 5. Typical examples of (a) unstable symmetric and (b) stable asymmetric modes, produced by both the VA and numerical solution of Eq. (7) for $\varepsilon = 3$ and $N = 10$. The respective energy eigenvalues are (a) $\mu_{\rm VA} = -3.53$ and $\mu_{\rm num} = -4.39$ and (b) $\mu_{\rm VA} = -10.04$ and $\mu_{\rm num} = -12.90$.

while its asymmetry at $b \neq 0$ is quantified by the parameter (10),

$$\Theta = \frac{16}{15\pi}\frac{b(5a-3c)}{a^2+c^2+b^2}. \tag{31}$$

A straightforward consideration confirms that the expression (31) is always subject to the constraint $|\Theta| < 1$, as it must be. The Sturm theorem, according to which the spatially symmetric g.s. cannot have nodes [1], i.e., $\phi(x) \neq 0$ at $|x| < 1/2$ (it remains valid in the nonlinear system), if applied to the ansatz (29) with $b = 0$, amounts to the following constraint:

$$-1 < c/a < 1/3. \tag{32}$$

The substitution of the ansatz (29) into the Lagrangian (28) yields

$$\begin{aligned} L_{\rm VA} = {} & \left(\tfrac{1}{4}\pi^2 - \tfrac{1}{2}\mu + \varepsilon\right)a^2 + \left(\pi^2 - \tfrac{1}{2}\mu\right)b^2 \\ & + \left(\tfrac{9}{4}\pi^2 - \tfrac{1}{2}\mu + \varepsilon\right)c^2 + 2\varepsilon ac - \tfrac{1}{4}\left(\tfrac{3}{4}a^4 + a^3c + 3a^2b^2 \right. \\ & \left. + 3a^2c^2 - 3ab^2c + \tfrac{3}{4}b^4 + 3b^2c^2 + \tfrac{3}{4}c^4\right), \end{aligned} \tag{33}$$

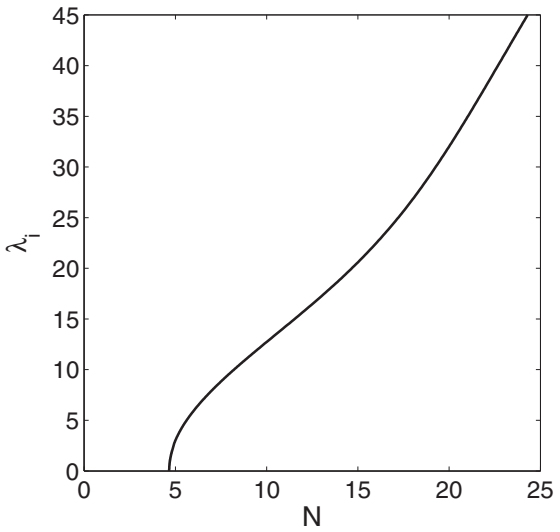


FIG. 6. Instability growth rate $\lambda_{\rm i} \equiv {\rm Im}(\lambda)$ of small perturbations added to the unstable symmetric mode at $\varepsilon = 3$ and $N > N_{\rm bif}$ [see Eq. (41)]. The growth rate was found as a numerical solution of Eq. (42). The instability sets in at exactly the same bifurcation point at which the SSB starts in Fig. 4(a).

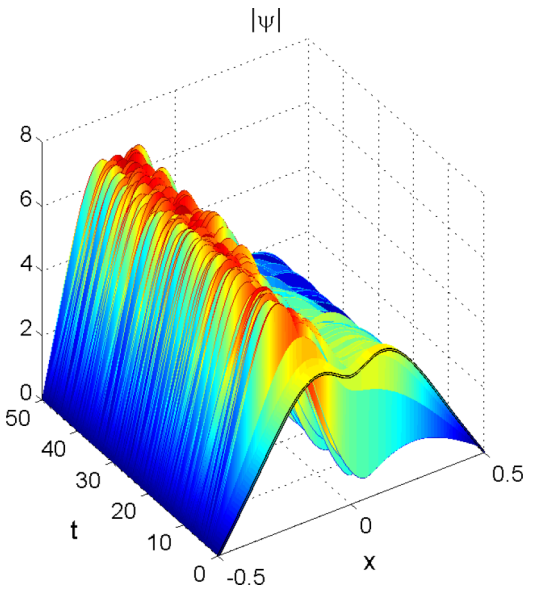


FIG. 7. Typical example of the spontaneous conversion of a perturbed unstable symmetric mode into a stable asymmetric one, at $\varepsilon = 3$, $\mu = 3$, and $N = 10.39$.

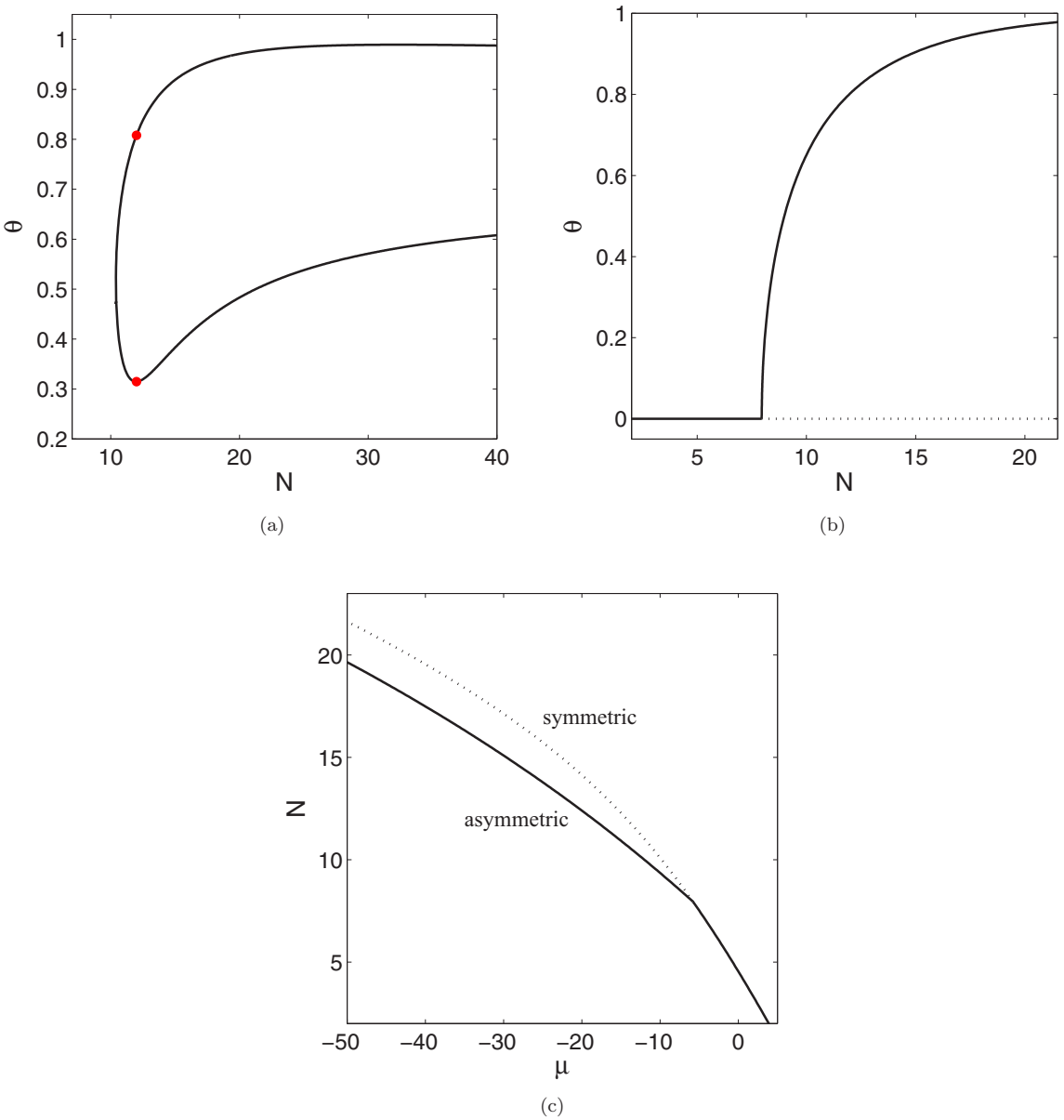


FIG. 8. (a) Bifurcation diagram shown by means of the $\Theta(N)$ dependence, as predicted by the VA at $\varepsilon = 1$. Red circles denote two asymmetric solutions for $N = 12$, shown in Fig. 9. (b) Counterpart of the bifurcation diagram from (a), as produced by the numerical solution of Eq. (7). (c) Numerically generated $N(\mu)$ dependences corresponding to (b).

which gives rise to the variational equations for the real amplitudes $b$ and $a$,$c$:

$$\partial L/\partial(b^2) = 0, \tag{34}$$

$$\partial L/\partial a = \partial L/\partial c = 0. \tag{35}$$

To identify the bifurcation point at which the SSB sets in, one may set $b = 0$ in Eqs. (34) and (35) [*after* performing the differentiation with respect to $b^2$ in Eq. (34)]. This procedure leads to a system of equations for the values of $a$, $c$, and $\mu$ at the bifurcation point:

$$2\pi^2 - \mu = \tfrac{3}{2}(a^2 - ac + c^2), \tag{36}$$

$$\left(\tfrac{1}{2}\pi^2 - \mu + 2\varepsilon\right)a + 2\varepsilon c - \tfrac{1}{4}(3a^3 + 3a^2c + 6ac^2) = 0, \tag{37}$$

$$\left(\tfrac{9}{2}\pi^2 - \mu + 2\varepsilon\right)c + 2\varepsilon a - \tfrac{1}{4}(a^3 + 6a^2c + 3c^3) = 0. \tag{38}$$

It is easy to check that Eqs. (36)–(38) have no relevant solutions at $\varepsilon = 0$, in agreement with the obvious fact that the SSB does not occur when the central barrier is absent, i.e., the potential box is not split into two wells.

The VA-produced prediction for the bifurcation point, in the form of $N_{\rm bif}(\varepsilon)$, obtained from a numerical solution of Eqs. (36)–(38), is compared to its numerically found counterpart in Figs. 2(a) and 2(b). It can be seen that the VA provides reasonable accuracy at moderate values of $\varepsilon$. At large $\varepsilon$, the discrepancy is explained by the fact that the ansatz

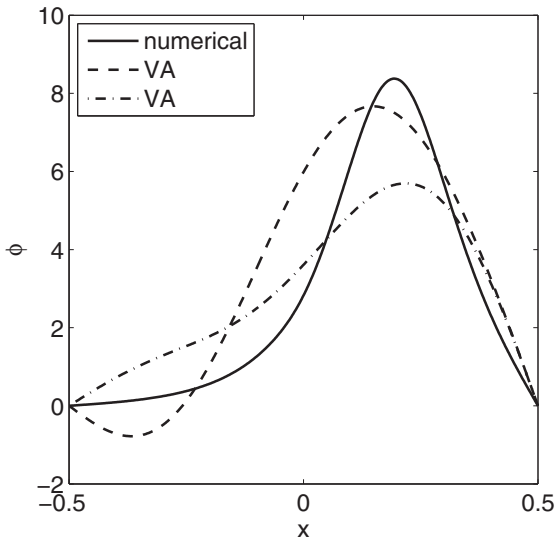


FIG. 9. Dashed and dash-dotted profiles represent the VA-predicted asymmetric solutions corresponding, respectively, to the top and bottom red circles in Fig. 8(a), obtained at $\varepsilon = 1$ and $N = 12$. The solid profile depicts the solution obtained from the numerical solution of Eq. (7) with the same parameters. The values of the energy eigenvalue pertaining to the dashed, dash-dotted, and solid profiles are $\mu = -24.7$, $-20.7$, and $-32.0$, respectively.

(29) does not take into account the derivative's jump given by Eq. (8). On the other hand, at very small $\varepsilon$, the relevant ansatz is also different, as it amounts to the soliton (22).

Equations (37) and (38), in which the cubic terms are dropped [and Eq. (36) is dropped too], correspond to the linearized version of Eq. (7), with $g = 0$. This simplest version of the VA predicts the above-mentioned eigenvalue $\mu_0(\varepsilon)$, which corresponds to the g.s. of the linear system, as a value at which the determinant of the linearized version of Eqs. (37) and (38) for $a$ and $c$ vanishes:

$$(\mu_0)_{\rm VA} = \tfrac{5}{2}\pi^2 + 2\varepsilon - 2\sqrt{\pi^4 + \varepsilon^2} \tag{39}$$

[recall that Eq. (12) for $\mu(\varepsilon)$ cannot be solved exactly, except for concluding that $\mu_0$ is a monotonically growing function of $\varepsilon$ confined to the interval $\pi^2/2 \leqslant \mu_0 < 2\pi^2$; see Eqs. (13) and (20)]. In particular, the approximate g.s. energy, produced by Eq. (39), satisfies the constraint $\mu_0 < 2\pi^2$ at $\varepsilon < (15/8)\pi^2 \approx 18.5$. This approximate result is compared to its numerical counterpart in Fig. 3. As mentioned above, the discrepancy at large $\varepsilon$ is explained by the fact that the ansatz (29) does not take into account the jump of the derivative at $x = 0$. The predictions of the VA are further compared with numerical findings in the next section.

## III. NUMERICAL RESULTS

Numerical solutions of Eqs. (3) and (7) were obtained by replacing the ideal $\delta$ function with its regularized version

$$\tilde{\delta}(x) = \frac{1}{\sqrt{\pi}\xi} \exp\left(-\frac{x^2}{\xi^2}\right), \tag{40}$$

with width $\xi \ll 1$ (the results are presented below for $\xi = 0.05$; at still smaller values of the regularization width, such as $\xi = 0.01$, the findings are essentially the same). Solutions of the stationary equation (7) were produced by means of the Newton's method, with mesh size $\Delta x = 1/1025$. Direct simulations of the evolution governed by Eq. (3) were performed by the standard split-step algorithm, with time step $\Delta t = 0.001$.

The stability of the stationary modes was explored through a numerical solution of the GPE linearized for small perturbations around the stationary mode. For this purpose, the perturbed version of stationary solutions (6) is taken in the usual form

$$\psi(x,t) = e^{-i\mu t}\{\phi(x) + \eta[e^{-i\lambda t}u(x) + e^{i\lambda^* t}v^*(x)]\}, \tag{41}$$

where $\eta$ is an infinitesimal amplitude of the perturbations, $u(x)$ and $v(x)$ represent an eigenmode, and $\lambda$ is the corresponding (generally, complex) perturbation eigenfrequency, the stability condition being $\mathrm{Im}\{\lambda\} = 0$ for all $\lambda$. The substitution of the expression (41) in Eqs. (3) and (4) and the subsequent linearization gives rise to the eigenvalue problem for $\lambda$, based on the following equations:

$$\begin{aligned} (\mu + \lambda)u + \tfrac{1}{2}u'' + g\phi^2(x)(2u + v) &= \varepsilon\delta(x)u, \\ (\mu - \lambda)v + \tfrac{1}{2}v'' + g\phi^2(x)(2v + u) &= \varepsilon\delta(x)v, \\ u\left(x = \pm\tfrac{1}{2}\right) = v\left(x = \pm\tfrac{1}{2}\right) &= 0, \end{aligned} \tag{42}$$

with the prime standing for $d/dx$. Equations (42) were solved numerically [with $g = 1$ and $\delta(x)$ replaced by $\tilde{\delta}(x)$, as per Eq. (40)] by means of the finite-difference method. Predictions for the instability or stability of stationary modes, produced by the linearized GPE, were verified by means of direct simulations of their perturbed evolution in the framework of the full equation (3).

### A. Symmetric and asymmetric modes and SSB at moderate values of $\varepsilon$

For $\varepsilon$ that is not too small, both the numerical solution of the VA equations (34) and (35) and the numerical solution of the stationary GPE (7) give rise to a characteristic picture of the *supercritical bifurcation* [8], which is displayed in Fig. 4(a), showing the asymmetry, defined as per Eqs. (9) and (10), versus the total norm. In a broad range of values of $\varepsilon$ [provided that it is not too small (see below)], this diagram, as predicted by the VA through Eq. (31), is virtually identical to its numerical counterpart.

The solution of the VA equations (34) and (35) also predicts $N(\mu)$ dependences for the symmetric and asymmetric solutions, which are displayed and compared to their GPE-produced counterparts in Fig. 4(b). It can be seen that the discrepancy is larger than in the bifurcation diagram in Fig. 4(a), but, still, the VA provides reasonable accuracy.

As concerns particular profiles of the symmetric and asymmetric modes, produced by the VA and numerical solution of Eq. (7), typical examples, displayed in Fig. 5, demonstrate reasonable agreement between both. The remaining discrepancies between the variational and numerical profiles can be further reduced if more spatial harmonics are added to the ansatz (29), at the cost of making the VA equations (34) and (35) more cumbersome.

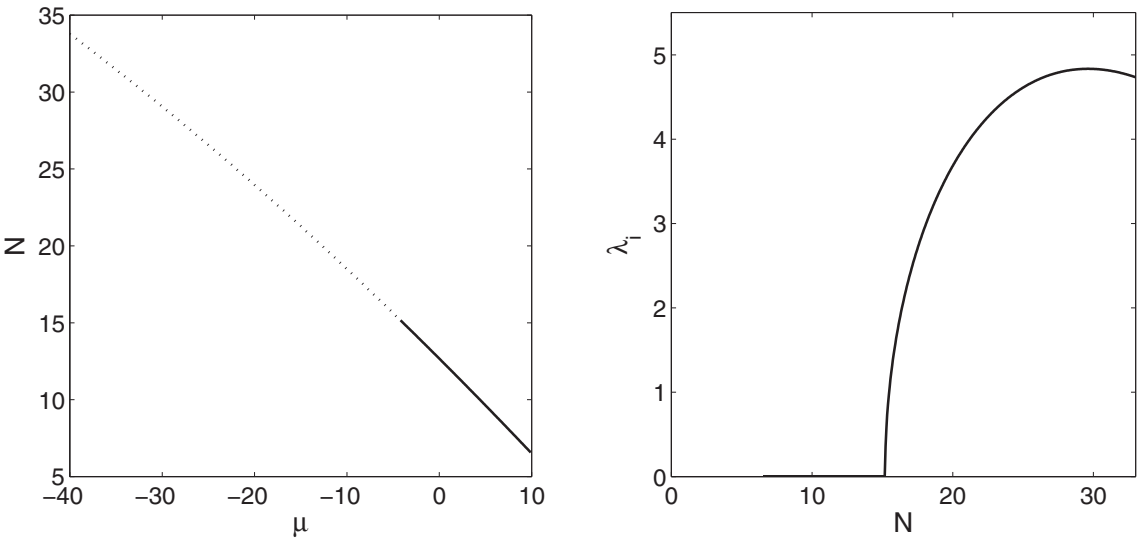


FIG. 10. (a) Numerically generated $N(\mu)$ dependence for the family of odd (antisymmetric) modes at $\varepsilon = 3$. Stable and unstable subfamilies are represented by the continuous and dotted segments, respectively. (b) Instability growth rate [see Eq. (41)] for the unstable portion of the family versus $N$.

Another conclusion following from Fig. 4(b) is that the branches of the $N(\mu)$ dependence satisfy the Vakhitov-Kolokolov criterion $dN/d\mu < 0$, which is a necessary (but not sufficient) condition for stability of localized modes supported by any self-attractive nonlinearity [9,31,32]. As concerns the full stability, it was checked, as mentioned above, by means of the numerical solution of the eigenvalue problem based on Eq. (42) and by direct simulations of Eq. (3) as well, the conclusion being typical for the supercritical bifurcation [7,8]: The symmetric mode at $N < N_{\rm bif}$ and the asymmetric ones at $N > N_{\rm bif}$ are stable, while the symmetric branch is unstable at $N > N_{\rm bif}$, when it coexists with the asymmetric counterparts.

The instability of the symmetric branch at $N > N_{\rm bif}$ is characterized, in Fig. 6, by the dependence of the respective growth rate Im(λ) [see Eq. (41)] on $N$. A typical example of the evolution of unstable symmetric modes is displayed in Fig. 7, which clearly shows a trend to conversion of this unstable mode into its stable asymmetric counterpart, with the same norm.

### B. SSB at small $\varepsilon$

The situation is different at smaller values of strength $\varepsilon$ of the splitting barrier. Namely, the direct numerical solution demonstrates that the SSB bifurcation keeps its supercritical

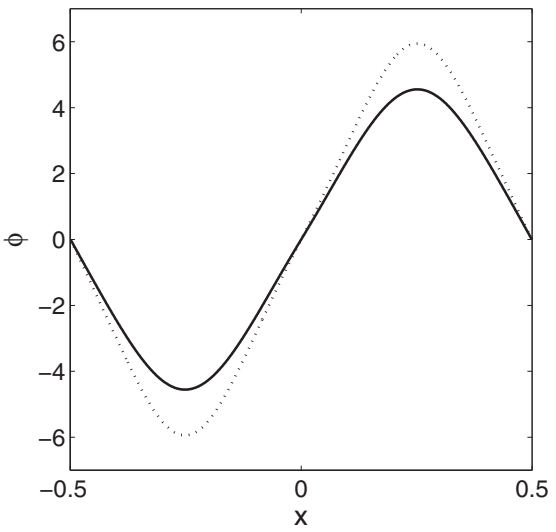


FIG. 11. Examples of stable and unstable (shown by the solid and dotted lines, respectively) odd modes, for $\varepsilon = 3$. The respective values of the norm and energy eigenvalue are $N = 9.63$ and $\mu = +5$, and $N = 15.63$ and $\mu = -5$.

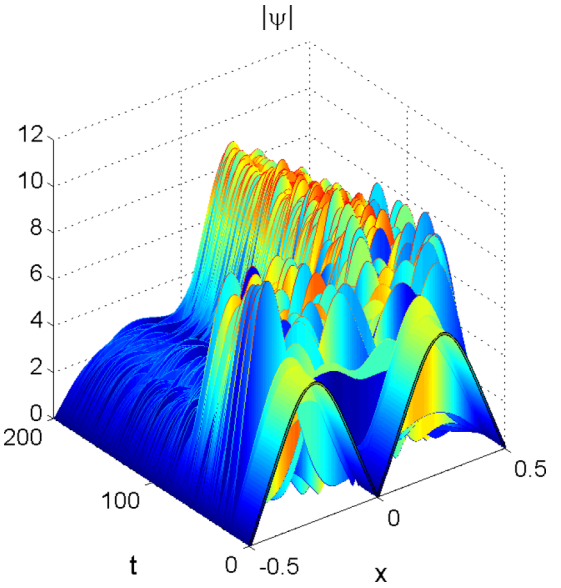


FIG. 12. Example of the spontaneous evolution of an unstable odd mode, shown by the dotted line in Fig. 11 (for $\varepsilon = 3$, $N = 15.63$, and $\mu = -5$), towards a stable asymmetric state.

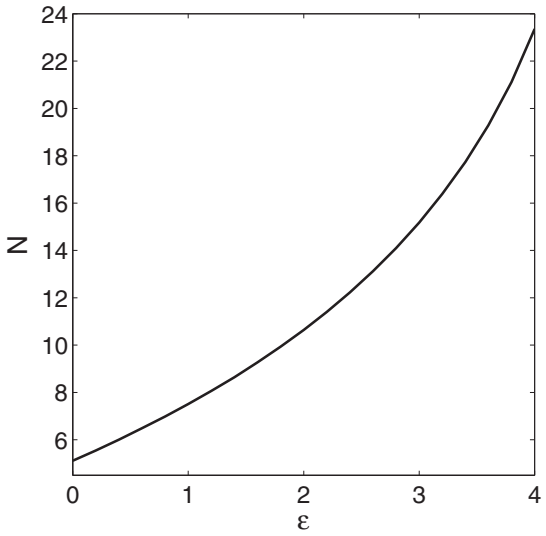


FIG. 13. Antisymmetric (odd) modes, which are the lowest excited states, are stable in the region below the boundary shown here in the plane of $(\varepsilon, N)$.

character, while the VA predicts a drastic change of the bifurcation diagram: detachment of the asymmetric branch from the symmetric one, at $\varepsilon < \varepsilon_{\rm cr}^{\rm (VA)} \approx 1.50$, as shown in Fig. 8 for $\varepsilon = 1$. In fact, a comparison of Figs. 8(a) and 8(b) demonstrates that the top branch of the $\theta(N)$ dependence is correctly predicted by the VA, while the bottom branch, which formally demonstrates the detachment of the asymmetric modes from the symmetric ones, is an artifact.

The partly wrong shape of the bifurcation diagram predicted by the VA in the case of $\varepsilon < \varepsilon_{\rm cr}^{\rm (VA)}$ is explained by the inadequacy of the ansatz (29) in this case. Indeed, a comparison of typical shapes of the asymmetric solutions produced by the VA with their numerically generated counterpart, shown in Fig. 9, demonstrates that the variational ansatz predicts the solutions belonging to the top branch of the bifurcation diagram [see Fig. 8(a)] in a qualitatively correct form, while the solutions belonging to the bottom branch have no numerically found counterparts, being an artifact of the VA. On the other hand, it is relevant to stress that the other analytical approximation, based on the soliton ansatz (22) and (24), correctly demonstrates that the supercritical SSB bifurcation occurs at small $\varepsilon$ too.

### C. Excited modes

As mentioned above, the shape of the first (spatially antisymmetric, or odd) excited mode in the model based on Eq. (1), with the ideal $\delta$-functional splitting barrier, is not affected by the barrier. However, stability of the antisymmetric mode against antisymmetry-breaking perturbations may be altered in the presence of the barrier. We have addressed this issue by means of the numerical analysis, replacing the ideal $\delta$ function with its regularized counterpart (40).

As shown in Fig. 10, it was found that the odd modes are stable if their norm is small enough and become unstable when $N$ exceeds a certain critical value; however, the instability is oscillatory, not being related to any antisymmetry-breaking bifurcation. Examples of stable and unstable odd modes are displayed in Fig. 11, with a typical scenario of the evolution of an unstable one presented in Fig. 12. It is observed that unstable odd modes tend to spontaneously transform themselves into stable asymmetric modes existing at the same value of $N$.

Results of the systematic analysis of the odd modes are collected in Fig. 13, which shows their instability threshold (in terms of the norm) versus $\varepsilon$. It can be seen that the stability interval of the odd modes is smallest ($N < N_{\rm cr} \approx 5.12$) in the absence of the splitting barrier, i.e., at $\varepsilon = 0$. The increase of $\varepsilon$ leads to expansion of the stability range, which may be explained by the following argument. In the case when both

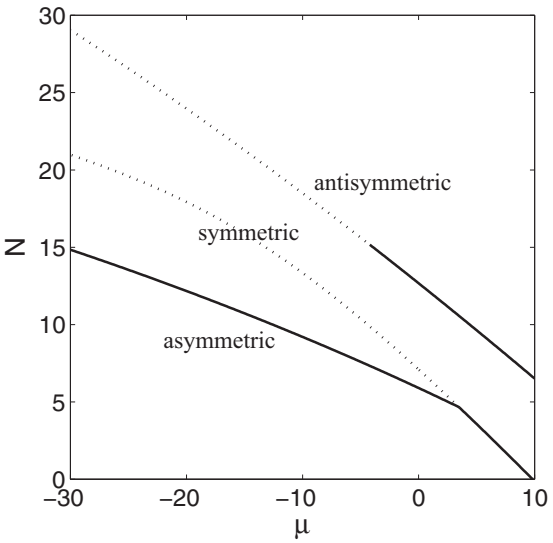


(a)

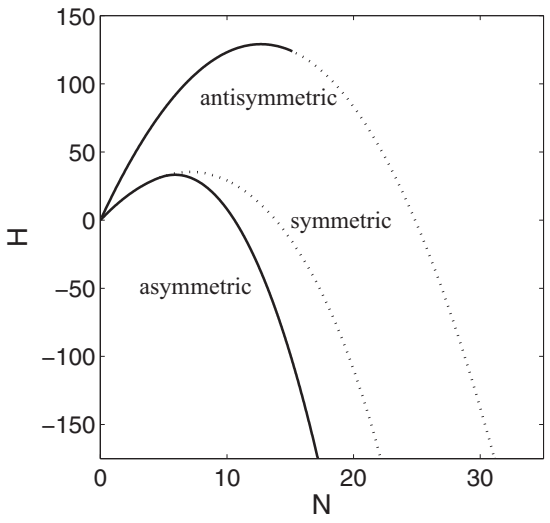


(b)

FIG. 14. (a) Juxtaposed $N(\mu)$ dependences for the symmetric (even), antisymmetric (odd), and asymmetric modes at $\varepsilon = 3$. (b) Hamiltonian versus the norm for the same modes, calculated as per Eqs. (5) and (43). In both panels, solid and dotted segments represent stable and unstable solutions, respectively.

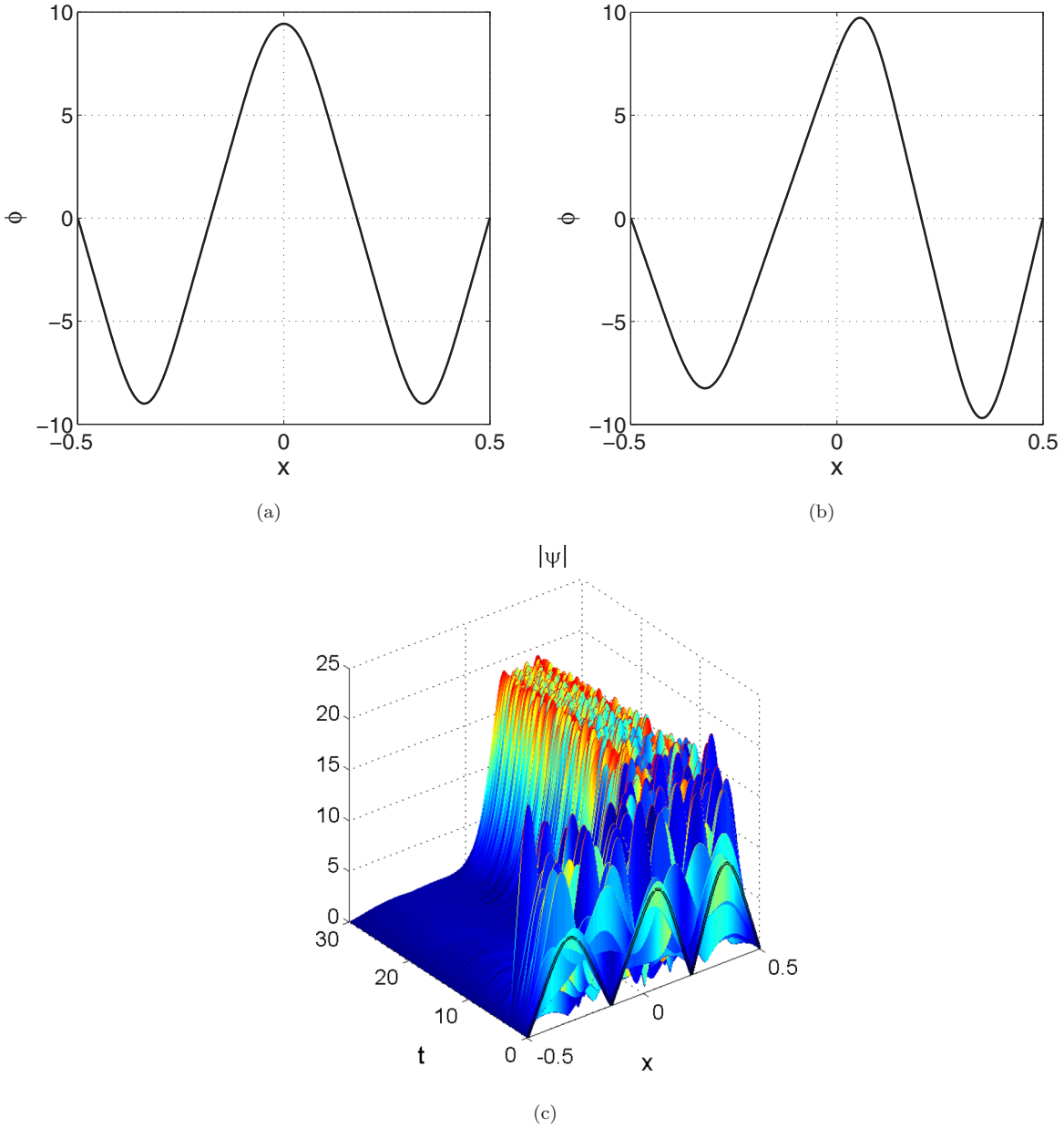


FIG. 15. Numerically found second excited states, as solutions of Eq. (7), for $\varepsilon = 3$ and $\mu = -10$: (a) a symmetric one, with norm $N = 38.13$ and (b) an asymmetric mode, with $N = 37.39$. (c) Numerically simulated evolution of the unstable asymmetric mode from (b).

$\varepsilon$ and $N$ are large, the odd mode may be considered as a superposition of two narrow half solitons (22), with norms $N \to N/2$, opposite signs, and centers located at opposite points $\pm\xi$. Because the energy of the free soliton, determined by Eq. (5), is $-(1/3)(N/2)^3$, the instability of the odd state against the merger of the two half solitons into a single one with norm $N$, placed in either half box (i.e., the instability against the breaking of the antisymmetry), is driven by the respective energy difference $\Delta E = N^3/4$. On the other hand, Eq. (26) suggests that, to pass the separating hurdle on the way to the merger, a half soliton must overcome an energy barrier of height $U_{\text{barrier}} \sim \varepsilon N^2$. Thus, the value of the norm at the instability threshold may be estimated, from the condition $\Delta E \sim U_{\text{barrier}}$, as $N_{\text{cr}} \sim \varepsilon$. Eventually, in the limit of $\varepsilon \to \infty$, the infinitely tall barrier splits the potential box into two isolated ones, each lobe of the odd mode carrying over into a stable g.s. of the half box, which implies that $N_{\text{cr}}(\varepsilon) \to \infty$ at $\varepsilon \to \infty$.

Because the odd modes are stable at sufficiently small values of $N$, it makes sense to compare their stability region with that of their symmetric and asymmetric counterparts. Figure 14(a) presents the comparison for $\varepsilon = 3$. Further, to identify the system's g.s., Fig. 14(b) displays the comparison of their Hamiltonian values as functions of the norm. The Hamiltonian is calculated according to Eq. (5), in which the last term is replaced as per Eq. (40):

$$\varepsilon|\psi(x=0)|^2 \to \varepsilon \int_{-1/2}^{+1/2} \tilde{\delta}(x)|\psi(x)|^2 dx. \tag{43}$$

It can be clearly seen that the odd mode is always an excited state, whose Hamiltonian exceeds that of the coexisting (for the same $N$) stable symmetric or asymmetric mode. Thus, the symmetric state, when it is stable, and the asymmetric one, when it exists, represent the g.s.

Finally, we have also carried out a brief analysis for the second excited state, i.e., the first even state existing above the g.s. In addition to the g.s., this mode undergoes the SSB, which gives rise, above the respective bifurcation point, to coexisting symmetric and asymmetric versions of the second excited state [see a typical example in Figs. 14(a) and 14(b)]. However, a drastic difference from the g.s. is that not only the formally existing symmetric mode, but also the coexisting asymmetric one, produced by the SSB, is unstable, as shown in Fig. 15(c). As a result of its evolution, the unstable asymmetric second-order state spontaneously evolves towards a stable asymmetric g.s., which exists at the same norm.

## IV. CONCLUSION

The objective of this work was to carry out a systematic analysis of a basic one-dimensional model that is capable of grasping the SSB phenomenology. The model, which may be realized in BECs and nonlinear optics alike, was built as an infinitely deep potential box, split into two wells by a narrow ($\delta$-functional) barrier set at the center. The barrier's strength $\varepsilon$ is the single free parameter in the scaled version of the model. The SSB was predicted in it by means of two analytical approximations, which are valid in two limit cases, viz., for strong or weak splitting of the potential box by the central barrier. Another semianalytical approach, based on the VA, was developed in the generic case. Predictions of the analytical approximations were verified by means of comparison with systematically generated numerical results. It was inferred that the system always gives rise to supercritical SSB bifurcation of the g.s. The VA accurately predicted this finding at moderate values of $\varepsilon$, but failed to do it at small $\varepsilon$, due to the limited applicability of the underlying ansatz. However, the other analytical approximation for small $\varepsilon$, which is based on the soliton ansatz, correctly described that case. In addition to the g.s., the stability of the first and second excited states was investigated too. The former (a spatially odd mode) is destabilized at a critical value of the norm. The second-order excited state, as well as the g.s., features the SSB bifurcation, but, unlike the g.s., the asymmetric mode produced by this bifurcation is unstable. In direct simulations, all unstable modes tend to rearrange themselves into the symmetry-broken g.s. with the same norm.

As an extension of the work it may be interesting to consider its two-dimensional version for a square-shaped infinitely deep potential box, split by appropriate inner barriers, a new factor appearing in two dimensions being a possibility of the collapse of the trapped modes. The analysis of a two-component version of the system may be relevant too.

## ACKNOWLEDGMENTS

This work was supported in part by the joint program in physics between the National Science Foundation (US) and Binational Science Foundation (US-Israel), through Grant No. 2015616.

[1] L. D. Landau and E. M. Lifshitz, *Quantum Mechanics* (Nauka, Moscow, 1974).

[2] A. W. Snyder and J. Love, *Optical Waveguide Theory* (Kluwer Academic, Boston, 1983).

[3] R. Englman, *The Jahn-Teller Effect in Molecules and Crystals* (Wiley-Interscience, London, 1972).

[4] S. Giorgini, L. P. Pitaevskii, and S. Stringari, Theory of ultracold atomic Fermi gases, Rev. Mod. Phys. **80**, 1215 (2008); H. T. C. Stoof, K. B. Gubbels, and D. B. M. Dickrsheid, *Ultracold Quantum Fields* (Springer, Dordrecht, 2009).

[5] A. E. Muryshev, G. V. Shlyapnikov, W. Ertmer, K. Sengstock, and M. Lewenstein, Dynamics of Dark Solitons in Elongated Bose-Einstein Condensates, Phys. Rev. Lett. **89**, 110401 (2002); L. Salasnich, A. Parola, and L. Reatto, Effective wave equations for the dynamics of cigar-shaped and disk-shaped Bose condensates, Phys. Rev. A **65**, 043614 (2002).

[6] Y. S. Kivshar and G. P. Agrawal, *Optical Solitons: From Fibers to Photonic Crystals* (Academic, San Diego, 2003).

[7] Edited by B. A. Malomed, *Spontaneous Symmetry Breaking, Self-Trapping, and Josephson Oscillations* (Springer, Berlin, 2013).

[8] G. Iooss and D. D. Joseph, *Elementary Stability Bifurcation Theory* (Springer, New York, 1980).

[9] E. A. Kuznetsov and F. Dias, Bifurcations of solitons and their stability, Phys. Rep. **507**, 43 (2011).

[10] E. B. Davies, Symmetry breaking in a non-linear Schrödinger equation, Commun. Math. Phys. **64**, 191 (1979); J. C. Eilbeck, P. S. Lomdahl, and A. C. Scott, The discrete self-trapping equation, Physica D **16**, 318 (1985); A. W. Snyder, D. J. Mitchell, L. Poladian, D. R. Rowland, and Y. Chen, Physics of nonlinear fiber couplers, J. Opt. Soc. Am. B **8**, 2102 (1991).

[11] G. L. Alfimov, P. G. Kevrekidis, V. V. Konotop, and M. Salerno, Wannier functions analysis of the nonlinear Schrödinger equation with a periodic potential, Phys. Rev. E **66**, 046608 (2002).

[12] P. G. Kevrekidis, Z. Chen, B. A. Malomed, D. J. Frantzeskakis, and M. I. Weinstein, Spontaneous symmetry breaking in photonic lattices: Theory and experiment, Phys. Lett. A **340**, 275 (2005).

[13] T. Heil, I. Fischer, W. Elsässer, J. Mulet, and C. R. Mirasso, Chaos Synchronization and Spontaneous Symmetry-Breaking in Symmetrically Delay-Coupled Semiconductor Lasers, Phys. Rev. Lett. **86**, 795 (2001).

[14] P. Hamel, S. Haddadi, F. Raineri, P. Monnier, G. Beaudoin, I. Sagnes, A. Levenson, and A. M. Yacomotti, Spontaneous mirror-symmetry breaking in coupled photonic-crystal nanolasers, Nat. Photon. **9**, 311 (2015); M. Marconi, J. Javaloyes, F. Raineri, A. Levenson, and A. M. Yacomotti, Stimulated scattering in strongly coupled nanolasers induced by Rabi oscillations, arXiv:1607.06753.

[15] M. Liu, D. A. Powell, I. V. Shadrivov, M. Lapine, and Y. S. Kivshar, Spontaneous chiral symmetry breaking in metamaterials, Nat. Commun. **5**, 4441 (2014).

[16] G. J. Milburn, J. Corney, E. M. Wright, and D. F. Walls, Quantum dynamics of an atomic Bose-Einstein condensate in a double-well potential, Phys. Rev. A **55**, 4318 (1997).

[17] A. Smerzi, S. Fantoni, S. Giovanazzi, and S. R. Shenoy, Quantum Coherent Atomic Tunneling Between two Trapped Bose-Einstein Condensates, Phys. Rev. Lett. **79**, 4950 (1997).

[18] M. Albiez, R. Gati, J. Fölling, S. Hunsmann, M. Cristiani, and M. K. Oberthaler, Direct Observation of Tunneling and Nonlinear Self-Trapping in a Single Bosonic Josephson Junction, Phys. Rev. Lett. **95**, 010402 (2005).

[19] G. Schön and A. D. Zaikin, Quantum coherent effects, phase transitions, and the dissipative dynamics of ultra small tunnel junctions, Phys. Rep. **198**, 237 (1990).

[20] A. V. Ustinov, Solitons in Josephson junctions, Physica D **123**, 315 (1998).

[21] S. Raghavan, A. Smerzi, S. Fantoni, and S. R. Shenoy, Coherent oscillations between two weakly coupled Bose-Einstein condensates: Josephson effects, $\pi$ oscillations, and macroscopic quantum self-trapping, Phys. Rev. A **59**, 620 (1999).

[22] H. E. Nistazakis, B. A. Malomed, P. G. Kevrekidis, and D. J. Frantzeskakis, Control of the symmetry breaking in double-well potentials by the resonant nonlinearity management, Chaos **21**, 013114 (2011).

[23] K. B. Zegadlo, N. Dror, M. Trippenbach, M. A. Karpierz, and B. A. Malomed, Spontaneous symmetry breaking of self-trapped and leaky modes in quasi-double-well potentials, Phys. Rev. A **93**, 023644 (2016).

[24] E. Ott, *Chaos in Dynamical Systems* (Cambridge University Press, Cambridge, 1993).

[25] B. A. Malomed, Symmetry breaking in laser cavities, Nat. Photon. **9**, 287 (2015).

[26] B. A. Malomed, in *Nonlinear Dynamics: Materials, Theory and Experiments*, edited by M. Tlidi and M. Clerc, Springer Proceedings in Physics Vol. 173 (Springer, Berlin, 2016), pp. 97–112.

[27] J. Hukriede, D. Runde, and D. Kip, Fabrication and application of holographic Bragg gratings in lithium niobate channel waveguides, J. Phys. D **36**, R1 (2003).

[28] V. I. Karpman and V. V. Solov'ev, A perturbation approach to the 2-soliton systems, Physica D **3**, 487 (1981); J. P. Gordon, Interaction forces among solitons in optical fibers, Opt. Lett. **8**, 596 (1983); F. M. Mitschke and L. F. Mollenauer, Experimental observation of interaction forces between solitons in optical fibers, *ibid.* **12**, 355 (1987).

[29] Y. S. Kivshar and B. A. Malomed, Dynamics of solitons in nearly integrable systems, Rev. Mod. Phys. **61**, 763 (1989).

[30] B. A. Malomed, Variational methods in nonlinear fiber optics and related fields, Prog. Opt. **43**, 71 (2002).

[31] M. Vakhitov and A. Kolokolov, Stationary solutions of the wave equation in a medium with nonlinearity saturation, Radiophys. Quantum Electron. **16**, 783 (1973).

[32] L. Bergé, Wave collapse in physics: Principles and applications to light and plasma waves, Phys. Rep. **303**, 259 (1998).